

Resource Management and Circuit Scheduling for Distributed Quantum Computing Interconnect Networks

Sima Bahrani, Romerson D. Oliveira, Juan Marcelo Parra-Ullauri, Rui Wang, and Dimitra Simeonidou

Abstract—Distributed quantum computing (DQC) has emerged as a promising approach to overcome the scalability limitations of monolithic quantum processors in terms of computational capability. However, realising the full potential of DQC requires effective resource management and circuit scheduling. This involves efficiently assigning each circuit to a subset of quantum processing units (QPUs), based on factors such as their computational power and connectivity. In heterogeneous DQC networks with arbitrary connectivity topologies and non-identical QPUs, this becomes a complex challenge. This paper addresses resource management and circuit scheduling in such settings, with a focus on computing resource allocation in a quantum data center. We propose circuit scheduling algorithms based on Mixed-Integer Linear Programming (MILP). Our MILP model accounts for errors arising from inter-QPU communication. In particular, the proposed schemes consider key factors, including network topology, QPU capacities, and quantum circuit structure, to make efficient scheduling and allocation decisions. Simulation results demonstrate that our proposed algorithms significantly improve circuit execution time and scheduling efficiency (measured by makespan and throughput), while also reducing inter-QPU communication overhead, compared to a baseline random allocation strategy. This work provides valuable insights into resource management strategies for scalable and heterogeneous DQC systems.

Index Terms—Distributed quantum computing, Quantum networks, Resource allocation, Quantum Circuits Scheduling

I. INTRODUCTION

Q UANTUM computing has gained attention as a solution for tackling intractable problems, due to its capacity to solve them significantly faster than traditional computers. In recent years, there have been notable advancements in quantum hardware and control systems, leading to the development of noisy intermediate-scale quantum processing units (QPUs).

This work was supported by Engineering and Physical Sciences Research Council Quantum Communication Hub grant ref. EP/T001011/1, EPSRC Integrated Quantum Networks Hub grant EP/Z533208/1, and the Innovate UK-funded project, Quantum Data Centre of the Future (10004793). (Corresponding authors: Sima Bahrani and Rui Wang)

Sima Bahrani, Rui Wang, and Dimitra Simeonidou are with the Smart Internet Lab, School of Electrical, Electronic, and Mechanical Engineering, University of Bristol, Bristol, BS8 1UB, UK (e-mail: sima.bahrani@bristol.ac.uk; rui.wang@bristol.ac.uk; Dimitra.Simeonidou@bristol.ac.uk).

Romerson D. Oliveira was with the Smart Internet Lab, School of Electrical, Electronic, and Mechanical Engineering, University of Bristol, Bristol, BS8 1UB, UK, and is now with Nu Quantum, Cambridge, UK (e-mail: romerson.oliveira@nu-quantum.com).

Juan Marcelo Parra-Ullauri was with the Smart Internet Lab, School of Electrical, Electronic, and Mechanical Engineering, University of Bristol, Bristol, BS8 1UB, UK, and is now with BT, Bristol, UK (e-mail: juan.m.parraullauri@bt.com).

However, despite these efforts, current quantum processors still remain limited in their computational power [1], [2]. Distributed quantum computing aims to harness the collective power of multiple interconnected quantum processors, enabling the execution of larger and more complex quantum algorithms. In DQC, quantum algorithms are partitioned and executed across a network of quantum processors, which are interconnected through both quantum and classical communication channels. By distributing the computational workload among multiple quantum processors, this approach facilitates the development of scalable quantum computing systems that can surpass the limitations imposed by individual quantum processors [3], [4].

Distributed quantum computing is expected to progress through stages of increasing scale and heterogeneity [2]. This progression spans from the integration of multiple quantum processors within a single large quantum computer to the establishment of interconnected quantum processors across various quantum data centres. A quantum data centre, in this context, refers to a facility housing quantum computers and the infrastructure for their operation and maintenance at the scale of links ranging between tens and hundreds of meters, like a modern classical data centre.

One of the fundamental requirements for DQC is the ability to perform quantum operations between distant qubits located on separate QPUs, often referred to as *remote gates*. Most approaches for realising remote gates rely on three key components: remote entanglement generation, local quantum operations on individual QPUs, and classical communication between them [3], [5]. As an illustrative example, Fig. 1 shows the circuit diagram for implementing a controlled-NOT (CNOT) gate based on this approach between two *computing qubits*, denoted by q_{cp1} and q_{cp2} , belonging to separate QPUs (QPU_1 and QPU_2). The initial step in this method involves generating entanglement between two dedicated *communication qubits*, denoted by q_{cm1} and q_{cm2} in Fig. 1, which facilitates the quantum communication between the QPUs. As depicted in the figure, the X operation on QPU_2 and the Z operation on QPU_1 are conditioned on the measurement outcome transmitted classically from each other. The same approach can be extended to implement other controlled-unitary gates.

The integration of quantum networking, classical networking, and quantum computation within a DQC interconnect network requires efficient orchestration of various components and tasks. A critical element in this orchestration is quantum

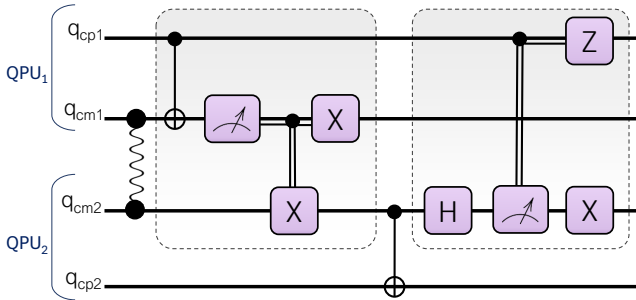


Fig. 1. Circuit diagram of remote CNOT gate performed between two QPUs.

compilation, which translates a high-level description of a quantum program into a set of instructions to be applied to the physical hardware [6], [7]. This translation is performed through several layers of subroutines forming a compilation stack, as depicted on the left of the Fig. 2. In the context of DQC, additional tasks must be executed for an intermediate representation of the quantum program, which we refer to as the *Quantum Circuit* (QCirc) (see right side of Fig. 2) in this work. These tasks involve various aspects of resource management, encompassing both network and compute resources. Compute resources primarily refer to the computing qubits embedded in QPUs, while communication resources include communication qubits and network components such as optical switches.

In this work, we focus on DQC within a single quantum data centre scale, where network and compute resource management are handled independently - a separation that improves scalability and modularity, both of which are essential in the complex DQC ecosystem and are consistent with the DQC architecture as described in [2]. Within this framework, the network is assumed to reliably establish entanglement links as needed to support remote operations between QPUs, and to allocate the required resources, including communication qubits, on demand. Accordingly, this work focuses on compute resource management, comprising two key stages: *circuit scheduling* and *circuit partitioning*. *Circuit scheduling* manages the queue of QCircs, determines the set of QPUs allocated to each QCirc, and addresses the QCirc-to-QPU mapping problem in the presence of multiple concurrent user requests. *Circuit partitioning* then optimises the division of each QCirc into smaller sub-circuits, taking into account the number of partitions, the specific QPUs assigned during scheduling, and the structure of the circuit.

Job scheduling in classical cloud data centres is a well-studied topic in the literature, typically focusing on criteria such as maximising resource utilisation, minimising makespan (total completion time of all tasks), and balancing the load across computing resources [8]–[11]. However, quantum computing introduces additional critical considerations. In particular, remote gate operations introduce infidelities that can adversely affect quantum computation tasks. These infidelities may arise from qubit decoherence during remote gate execution, as well as from imperfect remote entanglement generation between QPUs. Quantum-specific constraints, such as limited qubit coherence time, imply that circuit scheduling can directly impact not only execution time but also computa-

tional fidelity. Furthermore, prior studies [12] have shown that quantum circuits exhibit varying levels of sensitivity to errors arising from distributed execution. Therefore, a scheduling policy that accounts for these quantum-specific challenges can significantly enhance both system performance and overall computational fidelity. For example, sparsely connected circuits, those with relatively few two-qubit interactions, can often be allocated with minimal inter-QPU communication. In contrast, densely connected circuits might require careful mapping to avoid excessive remote gates. If a sparse circuit is scheduled and allocated first, it may occupy the most favourable QPUs, forcing subsequent dense circuits into fragmented and suboptimal allocations. This can increase inter-QPU communication overhead, extend job execution time, and ultimately create scheduling bottlenecks at the system level. These considerations motivate the need for scheduling strategies that jointly account for multiple circuits, rather than treating them independently.

While extensive research in the literature has addressed different aspects of DQC, such as network resource management, quantum compilation, and circuit partitioning, relatively fewer efforts have focused on compute resource management, particularly considering the impact of quantum circuit scheduling. Given the strong interdependencies among these tasks, we now review key related works across these areas to position our contribution in context. Resource management and scheduling in DQC have been considered in [13]–[16]. Nevertheless, these works primarily focus on network resource management, such as scheduling entanglement requests, quantum routing, and designing efficient entanglement generation or allocation protocols. In contrast, our work addresses compute resource management, specifically job (QCirc) scheduling and QPU–QCirc mapping in heterogeneous DQC networks.

Quantum compilation for DQC has been explored in several works. Ferrari et al. [17] discussed challenges in compiler design for DQC and analytically characterised the overhead introduced by remote gates. Cuomo et al. [18] proposed compilation techniques to optimise circuit execution time and distributed entangled state usage. They modeled time as additional circuit depth layers due to entanglement generation, but their approach assumes a uniform entanglement generation rate and neglects the dependency of network topology and associated loss. In a subsequent work, Ferrari et al. [19] presented a modular compilation framework incorporating network and QPU constraints. While this framework effectively considers network configuration and QPU characteristics, it primarily focuses on compilation and partitioning for a single circuit assigned to a fixed number of QPUs.

Circuit partitioning has also received significant attention. Daei et al. [20] represent QCircs as undirected graphs where qubits are nodes and edge weights correspond to the number of two-qubit gates shared between them. They then employ the Kernighan-Lin (K-L) algorithm to partition the graph, minimising the number of edges cut across partitions. In other studies [21]–[25], methods such as hypergraph partitioning, bipartite graph partitioning, window-based partitioning, and genetic algorithms have been employed to minimise the number of remote gates. Andres et al. [26] extended previous works

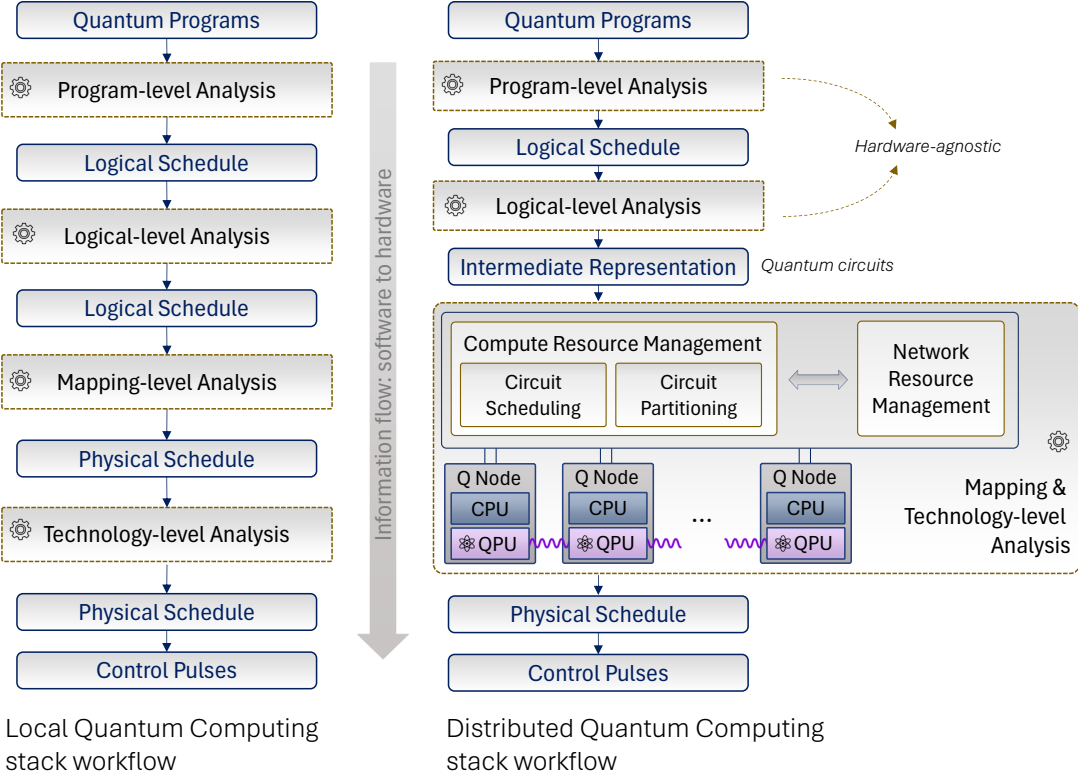


Fig. 2. Workflow of the quantum stack for both local and distributed quantum computing. A layered-oriented approach for compilation tools that bridge quantum algorithms with quantum devices. The stack workflow for local quantum computing, depicted on the left side of the figure, is based on [7].

on circuit partitioning to the case of heterogeneous networks with arbitrary topologies. While these studies have focused on optimally partitioning a single QCirc assuming a fixed number of partitions, they have not explicitly considered the issue of resource competition when multiple QCircs are to be concurrently assigned.

There exist gaps in DQC, particularly a lack of advanced QCirc scheduling algorithms that account for circuit partitioning when mapping and allocating resources for efficient distributed quantum computing. To the best of our knowledge, only Parekh et al. [27] proposed a greedy scheduling algorithm that assigns QCircs and fills QPUs on a one-by-one basis. However, their algorithm does not consider factors such as network topology and configuration, QPU decoherence properties, and the distinctive features of QCircs.

Here, we address the problem of QCircs scheduling in DQC networks, accounting for quantum-specific challenges such as fidelity degradation from remote operations. We adopt a general heterogeneous network model with QPUs of varying capacities, arbitrary connectivity topologies, and diverse QCircs. On this basis, we propose two scheduling algorithms: (i) a dynamic batch scheduling approach that leverages MILP to jointly optimise QPU–QCirc mapping and the number of circuit partitions for a batch of QCircs, and (ii) an MILP-based online scheduling strategy that allocates circuits individually. The proposed methods are extensively analysed and evaluated through detailed simulations.

The remainder of this paper is organised as follows. Sec. II

describes the DQC network model. Section III presents the proposed Batch-QCirc and Single-QCirc scheduling methods. Section IV evaluates the proposed methods through simulations. Finally, Section V concludes the paper.

II. DQC NETWORK MODEL

We investigate a DQC network within a quantum data centre, where QPUs are interconnected via both quantum and classical links. Promising architectures for such data centre networks will employ high-speed optical switches to dynamically establish quantum links between QPUs. Quantum information of stationary computing qubits can be encoded in photons via transducers, using degrees of freedom such as time-bin, polarization, frequency, etc [28], [29]. At the physical and link layers, remote entanglement between two QPUs can be generated in various ways [30], with one example illustrated in Fig. 3. This method relies on a Bell state measurement (BSM) module placed between the QPUs, enabling heralded entanglement generation. From an architectural perspective, switch-based data centre topologies such as fat-trees are promising candidates. A representative example with four pods is shown in Fig. 4(a), where QPUs are interconnected through three layers of optical switches to provide all-to-all connectivity. Alternatively, some designs may leverage entanglement swapping, allowing a QPU to act as a repeater and connect QPUs that are not directly linked.

At a higher abstracted connectivity level, the DQC network can be represented as in Fig. 4(b), which highlights the

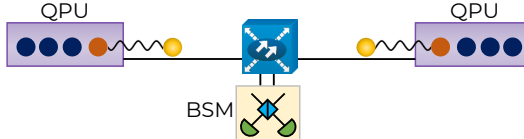


Fig. 3. High-level schematic of remote entanglement generation between a pair of QPUs via an intermediate BSM module. Blue circles denote computing qubits, and the brown circle denotes the communication qubit.

key components: QPUs connected by quantum and classical links, coordinated by a Quantum Network Controller. This abstraction captures the essential elements of the network while remaining agnostic to specific physical implementations and architectural details.

For our resource allocation and circuit scheduling problem, we further abstract the network into a logical graph model $G(V, E)$, where QPUs are represented as nodes and quantum logical links as edges. Each edge between QPU_{j_1} and QPU_{j_2} is characterised by two parameters: the remote gate execution time $T_{j_1 j_2}$ and the fidelity of remote entanglement generation $F_{j_1 j_2}$. This model relies on several simplifying assumptions. First, we assume on-demand entanglement generation: remote entanglement generation is initiated and completed at the start of each remote gate operation, and the resulting entangled pair is used immediately. This eliminates the need for long entangled-pair storage time. Second, we assume quantum communication latency and fidelity values are fixed for each logical link. In this work, we refer to the latency of a quantum communication link as the time required for one successful entanglement generation event between QPUs. Under these assumptions, remote gate execution time $T_{j_1 j_2}$ is influenced by the entanglement generation rate, which typically decreases with increasing link loss. For example, in the fat-tree topology depicted in Fig. 1, link loss increases with the number of optical switches in the path, thereby increasing remote gate execution time. Link's fidelity $F_{j_1 j_2}$ is similarly influenced by factors such as link loss and the specific entanglement generation protocol used.

We now turn to the key definitions and assumptions related to QPUs in our DQC network model. The set of QPUs in the network is denoted by $\mathcal{QP} = \{QPU_j\}_{j=1}^J$, where J represents the total number of QPUs in the network. In the graph model $G(V, E)$, the vertex set V corresponds to \mathcal{QP} , i.e., $V \equiv \mathcal{QP}$. The capacity of QPU_j , defined as its total number of computing qubits, is denoted by N_j . We also introduce a binary parameter s_j , which represents the current availability of QPU_j . Specifically, $s_j = 1$ if QPU_j is available, and $s_j = 0$ otherwise. We assume that all QPUs are based on the same technology and exhibit nearly identical decoherence properties, characterised by a common decoherence time parameter, T_{dec} . It is important to note that the concept of “decoherence time” is technology-dependent. For example, in superconducting-qubit systems, two parameters, energy relaxation time T_1 and dephasing time T_2 , are often reported; these can be combined into a single effective value, such as $\min(T_1, T_2)$ or $\frac{T_1 T_2}{T_1 + T_2}$, for modelling purposes.

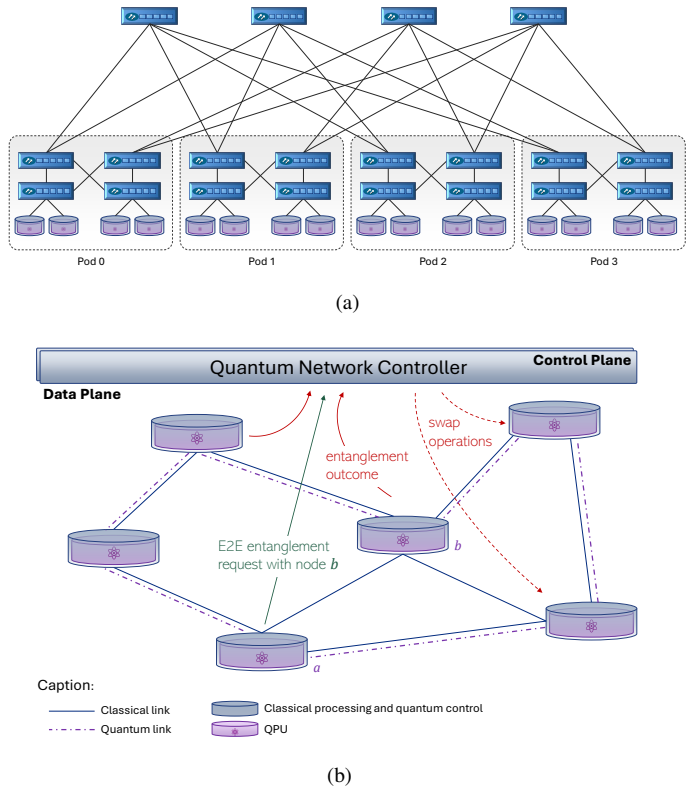


Fig. 4. (a) Example network architecture for a DQC network within a quantum data centre (fat-tree topology with 4 pods). (b) High-level abstract representation of the DQC network model.

In trapped-ion systems, a memory lifetime parameter may be used instead. Regardless of the specific definition, there always exists a parameter (or suitable combination thereof) that captures the temporal limitations imposed by decoherence. To maintain platform independence, we abstract this into a single representative parameter T_{dec} in our model.

III. PROPOSED QCIRC SCHEDULING METHODS

In this section, we consider the problem of QCirc scheduling for the DQC network described above. Our primary objective is to schedule a set of quantum circuits and allocate a subset of QPUs to each of them. The set of input quantum circuits is denoted by $\mathcal{QC} = \{QCirc_m\}_{m=1}^M$, where M is the total number of circuits. The required number of qubits for each circuit \mathcal{QC} is represented by w_m . We define K_m^{\max} as the maximum allowable number of partitions for $QCirc_m$, determined according to factors such as data centre policy, circuit size, or error tolerance. Throughout this work, we assume a non-preemption model, meaning that once a QCirc begins execution on its allocated QPUs, it runs to completion without interruption. Furthermore, each QPU can host at most one partition at any given time, meaning it cannot concurrently execute partitions from different circuits. In the following, we propose two primary QCirc scheduling methods. The first method, termed *Batch-QCirc Scheduling*, is based on dynamic batch scheduling, where a group of circuits is selected and assigned to QPUs collectively. The second

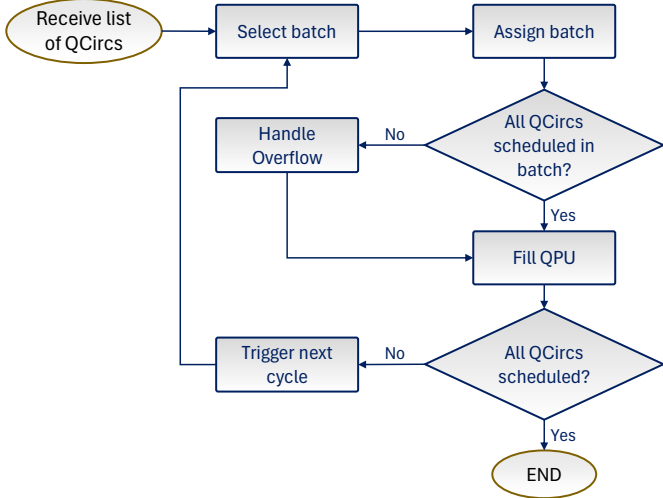


Fig. 5. Workflow of the Dynamic Batch-QCirc Scheduling method.

method, referred to as *Single-QCirc Scheduling*, assigns each circuit individually.

A. Dynamic Batch QCirc Scheduling

To efficiently schedule diverse quantum circuits (e.g. quantum Fourier transform), with varying qubit requirements and structures, we propose a batch scheduling framework that jointly optimises QPU allocation and the number of partitions for a batch of circuits. The algorithm operates in repeated scheduling cycles, each consisting of four main stages: (a) batch selection, where incoming quantum circuits are grouped into a batch based on their combined qubit requirements; (b) batch assignment, where the selected batch is mapped to available QPUs via a holistic MILP-based optimisation that accounts for decoherence effects and inter-QPU connectivity; (c) overflow handling, where any circuits that could not be assigned in the main step are promptly scheduled to run as soon as resources become available; and (d) filling idle QPUs, where any QPUs that remain unallocated after the batch assignment process are identified and, if suitable candidates exist in the remaining circuits of \mathcal{QC} , assigned to them, enhancing the utilisation of available resources.

The workflow for the proposed batch scheduling method is illustrated in Fig. 5, and the corresponding algorithm pseudocode is outlined in Algorithm 1. In each scheduling cycle, a batch of circuits is selected from \mathcal{QC} . This batch is denoted by $\mathcal{B} = \{\text{QCirc}_m \mid m \in \mathcal{I}\}$, where $\mathcal{I} \subseteq \{1, \dots, M\}$ is the set of indices corresponding to the selected circuits. The batch size, $S = |\mathcal{I}|$, may vary across scheduling cycles.

We adopt a simple batch selection process, where elements of \mathcal{QC} are sequentially added to \mathcal{B} based on their requests' arrival time until the total required number of qubits, $c_{\text{req}} = \sum_{m \in \mathcal{I}} w_m$, exceeds a threshold βc_{tot} . Here, c_{tot} denotes the total qubit capacity of all available QPUs, given by $c_{\text{tot}} = \sum_j s_j N_j$. The parameter β , fixed in the range $0 < \beta < 1$, is chosen to ensure that, with high probability, all circuits in the selected batch can be successfully assigned to available QPUs.

The selected batch then undergoes a batch assignment process, referred to as `ASSIGNBATCH` in Algorithm 1, where

Algorithm 1 Dynamic Batch-QCirc Scheduler

```

1: Input:  $\mathcal{QP}, \mathcal{QC}, G$ 
2: while not ISEMPTY( $\mathcal{QC}$ ) do
3:    $batch \leftarrow \text{SELECTBATCH}(\mathcal{QC}, \beta)$ 
4:    $batchMap \leftarrow \text{ASSIGNBATCH}(batch, \mathcal{QP}, G)$ 
5:   if not ALLASSIGNED( $batch$ ,  $batchMap$ ) then
6:     HANDLEOVERFLOW( $batch$ ,  $batchMap$ ,  $\mathcal{QP}$ )
7:   end if
8:   REMOVEASSIGNED( $\mathcal{QC}$ ,  $batch$ )
9:   if ANYAVAILABLE( $\mathcal{QP}$ ) then
10:    FILLQPU( $\mathcal{QC}$ ,  $\mathcal{QP}$ )
11:   end if
12:   TRIGGERNEXTCYCLE( $\mathcal{QP}$ ,  $\alpha$ )
13: end while
  
```

the circuits are mapped to the available QPUs. We have developed an MILP-based batch assignment algorithm, which will be described in detail in Sec. III-A1.

After the batch assignment, there might be a few circuits unassigned if the β is large, e.g., close to 1, or some circuits are complex to be distributed among available QPUs given the constraints. Any circuits in the batch that remain unassigned are handled after batch assignment using the `HANDLEOVERFLOW` procedure, described in Algorithm 2. The QPUs are first sorted in ascending order based on their expected busy time (EBT). The unassigned circuits are then assigned sequentially to the sorted QPUs, while taking into account circuit constraints such as capacity and the maximum number of partitions. The EBT for a given QPU can be estimated from the execution time of circuits already assigned to it or, when such information is not available, from other factors such as circuit connectivity, the number of partitions assigned to the circuit, and historical assignment data. This overflow step acts primarily as a failsafe, as β is chosen to make such cases rare.

To improve QPU utilisation, we incorporate a filling mechanism that assigns circuits to idle, unallocated QPUs. The `FILLQPU` algorithm, described in Algorithm 3, selects circuits from \mathcal{QC} and assigns each of them to idle QPUs individually, using a MILP-based optimisation strategy. To reduce the risk of excessive remote gate generation, only circuits with a ν_m value below a specified threshold are considered. Here, ν_m (also see in Sec. III-A1) is a score parameter that quantifies the circuit's connectivity and its likelihood of generating costly remote gates in a distributed setting. The MILP-based Single QCirc assignment process (`ASSIGNQCIRC` in Algorithm 3) is detailed in Sec. III-B.

Once all QPUs are allocated, the algorithm waits until a fraction α of the total qubit capacity across all QPUs, i.e., $\alpha \sum_j N_j$, becomes available, then proceeds to the next scheduling cycle. This mechanism is referred to as `TRIGGERNEXTCYCLE` in Algorithm 1.

1) *Batch-QCirc Assignment*: We propose an optimisation algorithm to minimise the detrimental effects of inter-QPU communication, focusing on decoherence-induced errors and fidelity loss from remote entanglement generation. Remote gates incur significantly higher execution time than local gates due to quantum and classical communication delays

Algorithm 2 HANDLEOVERFLOW

```

1: Input:  $batch, batchMap, \mathcal{QP}, G$ 
2:  $U \leftarrow$  Unassigned QCircs in  $batch$ 
3:  $\mathcal{QP}_s \leftarrow$  QPUs in  $\mathcal{QP}$  sorted by increasing EBT
4: for  $QCirc_m$  in  $U$  do
5:   Scan  $\mathcal{QP}_s$  to find a set  $\{QPU_{jk}\}_{k=1}^K$ 
   such that  $\sum_{k=1}^K N_{jk} \geq w_m$  and  $K \leq K_m^{\max}$ 
6:   Assign  $QCirc_m$  to  $\{QPU_{jk}\}_{k=1}^K$ 
7:    $\mathcal{QP}_s \leftarrow \mathcal{QP}_s \setminus \{QPU_{jk}\}_{k=1}^K \triangleright$  remove allocated QPUs
8: end for

```

Algorithm 3 FILLQPU

```

1: Input:  $\mathcal{QC}, \mathcal{QP}, G$ 
2:  $avlCapacity \leftarrow \sum_j N_j$  for idle QPUs
3: if  $avlCapacity > 0$  then
4:   for each  $QCirc_m$  in  $\mathcal{QC}$  do
5:     if  $\nu_m \leq \Gamma$  and  $w_m \leq avlCapacity$  then
6:       ASSIGNQCIRC( $QCirc_m$ )
7:       REMOVEASSIGNED( $QCirc_m$ )
8:       Update  $avlCapacity$ 
9:     end if
10:   end for
11: end if

```

and loss, increasing qubit exposure to decoherence. Moreover, remote entanglement generation is inherently imperfect, with fidelity that can degrade further through operations such as entanglement swapping and distillation. Repeated use of remote gates amplifies these effects, causing substantial fidelity loss and degrading the overall computational accuracy of distributed quantum computations. Our approach mitigates this degradation for the batch of QCircs as a group. The output of the Batch-QCirc assignment specifies the number of partitions assigned to each QCirc and the QPUs allocated for their execution, which then guide the circuit partitioning process in efficiently decomposing each QCirc into smaller sub-circuits. To mathematically formulate the problem of Batch-QCirc assignment, we begin by defining the following decision variables:

- Let r_{mj} be a binary variable, where $r_{mj} = 1$ if QPU_j is allocated to $QCirc_m$, and $r_{mj} = 0$ otherwise.
- Let y_{mk} be a binary variable, where $y_{mk} = 1$ if $QCirc_m$ is partitioned into exactly k parts (i.e., allocated to k distinct QPUs), and $y_{mk} = 0$ otherwise.

We define a cost function that captures the impact of qubit decoherence and imperfect entanglement generation during remote gate executions as follows:

$$C = \sum_{m \in \mathcal{I}} \sum_{k=1}^{K_m^{\max}} \sum_{1 \leq j_1 < j_2 \leq J} \nu_{mk} y_{mk} r_{mj_1} r_{mj_2} \left(\omega_0 \frac{w_m T_{j_1 j_2}}{T_{\text{dec}}} + \omega_1 (1 - F_{j_1 j_2}) \right) \quad (1)$$

where $T_{j_1 j_2}$ is the latency parameter, i.e., average time required to establish entanglement, associated with a remote gate between QPU_{j_1} and QPU_{j_2} , and $F_{j_1 j_2}$ is the fidelity parameter associated with remote entanglement generation for

TABLE I
LIST OF KEY NOTATIONS AND PARAMETERS

Parameter	Definition
$G(V, E)$	Graph representation of DQC network
\mathcal{QP}	Set of all QPUs
\mathcal{QC}	Set of all QCircs
\mathcal{B}	Selected batch of QCircs
J	Number of QPUs
M	Number of QCircs
S	Number of QCircs in the selected batch
T_{dec}	Decoherence time parameter of QPUs
N_j	Number of computing qubits within QPU_j
s_j	Equals to 1 if QPU_j is available, and 0 otherwise
w_m	Number of qubits required for $QCirc_m$
K_m^{\max}	partition count threshold for $QCirc_m$
r_{mj}	Equals to 1 if $QCirc_m$ is assigned to QPU_j , and 0 otherwise
y_{mk}	Equals to 1 if $QCirc_m$ is partitioned to k parts, and 0 otherwise
$T_{j_1 j_2}$	The latency parameter for establishing entanglement for remote gate execution, involving QPU_{j_1} and QPU_{j_2}
$F_{j_1 j_2}$	The fidelity parameter associated with remote entanglement generation between QPU_{j_1} and QPU_{j_2}
ν_{mk}	Partitioning cost coefficient for $QCirc_m$ and a given partition count k
g_m	Average degree of nodes in the graph model of $QCirc_m$
σ_m	Std. dev. of node degrees in the graph model of $QCirc_m$
$\lambda_{2,m}$	Algebraic connectivity of the graph model of $QCirc_m$
γ_m	Weighted density of the graph model of $QCirc_m$

the QPU pair. The term $(w_m T_{j_1 j_2})/T_{\text{dec}}$ captures the relative decoherence impact, where larger circuits (w_m) and longer communication delays ($T_{j_1 j_2}$) increase decoherence relative to the characteristic decoherence parameter T_{dec} . The parameters ω_0 and ω_1 are constant weights that reflect the relative importance of decoherence-induced errors versus fidelity loss from entanglement generation; unless otherwise stated, we set $\omega_0 = \omega_1$.

To incorporate circuit structure and connectivity patterns into our MILP objective, we introduce a partitioning cost coefficient ν_{mk} , which estimates the remote-gate overhead and thereby enables circuit-structure-aware resource allocation. Each quantum circuit is represented as a weighted undirected graph, where nodes correspond to qubits and edges correspond to two-qubit gates. The weight of each edge is given by the number of occurrences of gates between the respective qubit pair. Based on this representation, ν_{mk} is defined as the estimated graph cut size under k -way partitioning (with partitions of equal or nearly equal size). Although many distinct k -partitions are possible, adopting a standard balanced k -partition is sufficient to capture a circuit's connectivity level and its tendency to generate costly remote gates, while avoiding extra complexity.

To efficiently obtain ν_{mk} for different circuits without performing explicit graph partitioning, we propose an estimation method based on a linear regression model trained on three structural graph features: weighted density, algebraic connectivity, and coefficient of variance. This regression provides a lightweight estimate of cut size across circuit types, thereby making ν_{mk} tractable to compute in our MILP formulation. The three features are defined as follows:

- Weighted density** (γ_m) quantifies the average connec-

tivity per qubit pair, computed as

$$\gamma_m = \frac{\frac{1}{2} \sum_{i=1}^{w_m} g_m^{(i)}}{\binom{w_m}{2}}, \quad (2)$$

where $g_m^{(i)}$ denotes the weighted degree of qubit node i . The numerator corresponds to the total edge weight of the circuit graph, i.e., the total number of two-qubit gate occurrences across the circuit.

(ii) **Algebraic connectivity** ($\lambda_{2,m}$) is the second-smallest eigenvalue of the normalised Laplacian matrix L_m of the circuit graph [31]. It measures global connectivity strength; larger values indicate that the graph is harder to partition without cutting many edges.

(iii) **Coefficient of variance** (σ_m/g_m) captures connectivity imbalance across qubits, defined as

$$\frac{\sigma_m}{g_m} = \frac{\sqrt{\frac{1}{w_m} \sum_{i=1}^{w_m} (g_m^{(i)} - \bar{g}_m)^2}}{\frac{1}{w_m} \sum_{i=1}^{w_m} g_m^{(i)}}, \quad (3)$$

where \bar{g}_m and σ_m are the average and standard deviation of the weighted degrees $\{g_m^{(i)}\}$, respectively.

These features jointly capture complementary aspects of circuit structure: γ_m reflects the overall connectivity strength, particularly the density of pairwise interactions; $\lambda_{2,m}$ indicates how robustly the graph remains connected under partitioning; and σ_m/g_m captures connectivity imbalance across qubits that may create partitioning bottlenecks. Importantly, these features scale smoothly with circuit size w_m , enabling the simple but effective **linear regression model** to learn structural tendencies rather than raw size.

The regression target is the normalised k -way cut size:

$$\tilde{\nu}_{mk} = \frac{\text{Cut}_m^{(k)}}{\frac{1}{2} \sum_{i=1}^{w_m} g_m^{(i)}}, \quad (4)$$

where $\text{Cut}_m^{(k)}$ is the sum of edge weights for inter-partition edges when circuit m is optimally partitioned into k balanced parts. We then rescale by the total edge weight to recover the estimated partitioning cost coefficient:

$$\nu_{mk} \approx \left(\hat{\chi}_{0,k} \gamma_m + \hat{\chi}_{1,k} \lambda_{2,m} + \hat{\chi}_{2,k} \frac{\sigma_m}{g_m} + \hat{\chi}_{3,k} \right) \cdot \left(\frac{1}{2} \sum_{i=1}^{w_m} g_m^{(i)} \right). \quad (5)$$

Here, $(\hat{\chi}_{0,k}, \hat{\chi}_{1,k}, \hat{\chi}_{2,k}, \hat{\chi}_{3,k})$ denote the regression coefficients, which are pre-learned and fitted by minimising the mean squared error (MSE)

$$\frac{1}{|\mathcal{D}|} \sum_{d \in \mathcal{D}} \left(\tilde{\nu}_{dk} - \left(\hat{\chi}_{0,k} + \hat{\chi}_{1,k} \gamma_d + \hat{\chi}_{2,k} \lambda_{2,d} + \hat{\chi}_{3,k} \frac{\sigma_d}{g_d} \right) \right)^2, \quad (6)$$

for a given k partitions. In this expression, \mathcal{D} denotes a set of quantum circuits with varying types and qubit counts, and $\tilde{\nu}_{dk}$ is the normalised k -way cut size for circuit $d \in \mathcal{D}$.

Our optimisation problem, which minimises the cost function C in (1), is formulated as the MILP in Formulation 1. The cost function is linearised by introducing the auxiliary variables $z_{mj_1j_2} = r_{mj_1} r_{mj_2}$ and $x_{mkj_1j_2} = z_{mj_1j_2} y_{mk}$. The role of each constraint in Formulation 1 is as follows:

(1) **Minimum assignment:** Enforces a lower bound on the number of circuits scheduled in the current cycle. By default, $\zeta = M$ so that all circuits in the batch are assigned. If the MILP becomes infeasible, ζ is decremented until a feasible allocation is found.

(2) **Capacity requirement:** Ensures that the aggregate qubit capacity of the QPUs assigned to QCirc_m meets or exceeds its qubit requirement w_m . While s_j (QPU availability binary parameter) may vary between scheduling cycles, it is fixed within each cycle and thus treated as a parameter in the MILP.

(3) **Single-partition per QPU:** Ensures that each QPU is assigned at most one circuit partition in a scheduling cycle.

(4) **Link between binary variables:** Provides an MILP-compatible link between r_{mj} and y_{mk} .

(5)–(6) **Linearisation of $z_{mj_1j_2}$:** Implements MILP-compatible linear formulations of the equalities $z_{mj_1j_2} = r_{mj_1} r_{mj_2}$ and $x_{mkj_1j_2} = z_{mj_1j_2} y_{mk}$.

In the **FILLQPU** algorithm (Algorithm 3), we employ the parameter ν_{mk} as a scoring metric for circuit connectivity and remote-gate overhead estimation. In particular, we consider the case $k = 2$ (with the index k omitted in Algorithm 3 for simplicity), and only circuits with ν_m not exceeding a threshold Γ are selected for individual assignment.

Formulation 1. MILP-based Batch-QCirc assignment problem

$$\begin{aligned} \min \quad & \left\{ \sum_{m \in \mathcal{I}} \sum_{k=1}^{K_m^{\max}} \sum_{1 \leq j_1 < j_2 \leq J} \nu_{mk} x_{mkj_1j_2} \left(\omega_0 \frac{w_m T_{j_1j_2}}{T_{\text{dec}}} + \right. \right. \\ & \left. \left. \omega_1 (1 - F_{j_1j_2}) \right) \right\} \\ \text{s.t.} \quad & (1) \sum_{m \in \mathcal{I}} \sum_{k=1}^{K_m^{\max}} y_{mk} = \zeta \\ & (2) \sum_{j=1}^J r_{mj} s_j N_j \geq w_m \sum_{k=1}^{K_m^{\max}} y_{mk} \quad \forall m \in \mathcal{I} \\ & (3) \sum_{j=1}^J r_{mj} = \sum_{k=1}^{K_m^{\max}} k y_{mk} \quad \forall m \in \mathcal{I} \\ & (4) \sum_{m \in \mathcal{I}} r_{mj} \leq 1 \quad \forall j \\ & (5) r_{mj_1} + r_{mj_2} - 1 \leq z_{mj_1j_2} \leq r_{mj_1}, r_{mj_2} \\ & \quad \forall m \in \mathcal{I}, j_1 < j_2 \\ & (6) z_{mj_1j_2} + y_{mk} - 1 \leq x_{mkj_1j_2} \leq z_{mj_1j_2}, y_{mk} \\ & \quad \forall m \in \mathcal{I}, k, j_1 < j_2 \end{aligned}$$

B. Single-QCirc Scheduling

Another approach for scheduling quantum circuits is to schedule them individually rather than in batches. In this case, we propose a single-Qcirc scheduling algorithm, presented in pseudocode in Algorithm 4. This algorithm uses an

MILP-based assignment method to optimise QPU allocation for each circuit QCirc_m , taking into account the available QPUs, network topology, and link characteristics. The key difference from the batch-Qcirc scheduling method described in the previous subsection is that the batch approach jointly optimises allocation for all circuits in a batch, whereas the single-circuit method follows a one-by-one, online strategy that locally optimises each assignment. As a result, diversity in circuit structures and characteristics across the batch is not fully exploited in this method. On the other hand, the single-QCirc approach offers lower computational complexity and enables immediate scheduling of each circuit as soon as the required resources become available.

We adopt the same MILP-based framework to determine the optimal allocation for each circuit. This assignment procedure is referred to as **ASSIGNQCIRC** in Algorithm 4, and its MILP formulation is provided in Formulation 2. The same objective function and constraints from the batch formulation are used, but simplified for the single-circuit case. Note that **ASSIGNQCIRC** is also used within the **FILLQPU** procedure described in Algorithm 3.

Formulation 2. MILP-based Single-QCirc assignment problem

$$\begin{aligned} \min \quad & \left\{ \sum_{1 \leq j_1 < j_2 \leq J} z_{mj_1j_2} \left(\omega_0 \frac{w_m T_{j_1j_2}}{T_{\text{dec}}} + \omega_1 (1 - F_{j_1j_2}) \right) \right\} \\ \text{s.t.} \quad & \\ (1) \quad & \sum_{j=1}^J r_{mj} s_j N_j \geq w_m \quad \forall m \in \mathcal{I} \\ (2) \quad & \sum_{j=1}^J r_{mj} \leq K_m^{\max} \quad \forall m \in \mathcal{I} \\ (3) \quad & r_{mj_1} + r_{mj_2} - 1 \leq z_{mj_1j_2} \leq r_{mj_1}, r_{mj_2} \\ & \forall m \in \mathcal{I}, j_1 < j_2 \end{aligned}$$

IV. EVALUATION AND RESULTS

This section evaluates the proposed scheduling algorithms through simulations. We consider a DQC network consisting of 16 QPUs within a data centre. The QPUs have the following capacities: four QPUs with a capacity of 8 qubits, four with a capacity of 12 qubits, four with a capacity of 16 qubits, and four with a capacity of 20 qubits. These capacities are randomly assigned to individual QPUs using a fixed random seed

Algorithm 4 Single-QCirc Scheduler

```

1: Input:  $\mathcal{QC}$ ,  $\mathcal{QP}$ ,  $G$ 
2: while not IsEmpty( $\mathcal{QC}$ ) do
3:   for each  $\text{QCirc}_m$  in  $\mathcal{QC}$  do
4:     ASSIGNQCIRC( $\text{QCirc}_m$ )
5:     REMOVEASSIGNED( $\text{QCirc}_m$ )
6:   end for
7: end while

```

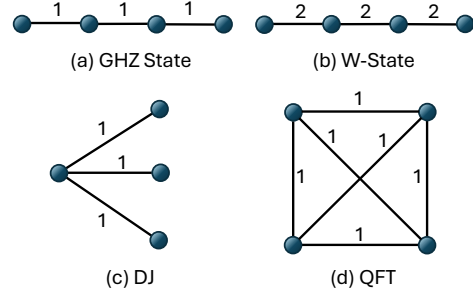


Fig. 6. Connectivity graphs for benchmark circuits ($w = 4$). Edge weights indicate the number of two-qubit gate occurrences.

to ensure consistent QPU configurations across all simulations. The entire simulation process is repeated for 10 different seed values, and the average results are presented.

The network adopts a fat tree topology of four pods with each pod consisting of 4 QPUs, as illustrated in Fig. 4(a). In Sec. II, we have defined two key parameters characterising the links in the logical topology: time required to establish entanglement ($T_{j_1j_2}$) and fidelity ($F_{j_1j_2}$) of entanglement generation for remote gates. Here, we specify their values for the 4-pod fat-tree topology used in our simulations. This topology features three types of links, distinguished by the number of optical switches along the path—specifically, 1, 3, or 5 switches. We denote the corresponding latency values by T_{link_1} , T_{link_3} , and T_{link_5} , respectively. Assuming an elementary link latency of T_{el} (corresponding to entanglement generation time between QPUs without loss from any optical switches), and noting that the entanglement generation rate is directly affected by link loss, thus the latency for each link type is calculated using the formula:

$$T_{\text{link}_{n_s}} = \frac{T_{\text{el}}}{\eta_s^{n_s}}, \quad (7)$$

where η_s is the switch transmission efficiency and $n_s \in \{1, 3, 5\}$ is the number of switches in the path. In our simulations, we assume that all optical switches are of the same type and have an identical loss of 0.5 dB. Given the short physical distances between QPUs in a data centre environment, propagation delays are considered negligible compared to the time needed for establishing entanglement. For the fidelity parameter, we assume a slight fidelity degradation with increasing link distance and loss, as follows: $F_{\text{link}_1} = 0.96$, $F_{\text{link}_3} = 0.94$, and $F_{\text{link}_5} = 0.92$.

To establish the set of quantum circuits \mathcal{QC} , we use benchmark circuits from the Munich Quantum Toolkit [32]: Quantum Fourier Transform (QFT), Deutsch–Jozsa (DJ), W-state, and GHZ-state circuits. Fig. 6 shows connectivity-graph representations for $w = 4$ qubits. From this figure, it can be inferred that GHZ and W-state circuits are sparsely connected, QFT circuits, modeled with a complete graph, are highly connected, and DJ circuits exhibit an intermediate level of connectivity. A set \mathcal{QC} of size M includes all four circuit types, with each type contributing 25% of the total. For circuit QCirc_m , the number of qubits w_m is randomly selected from a type-specific range. Two types of required qubit range are considered. In Scenario 1 (Sc.1), the ranges of required

TABLE II
LINEAR REGRESSION RESULTS FOR OUR BENCHMARK CIRCUITS
AND SIMULATION SCENARIOS.

	$\hat{\chi}_{0,k}$	$\hat{\chi}_{1,k}$	$\hat{\chi}_{2,k}$	$\hat{\chi}_{3,k}$	R^2 score
$k = 2$	0.0272	0.4345	0.0163	0.0434	0.9965
$k = 3$	0.1185	0.4808	0.0534	0.0802	0.9929
$k = 4$	0.1887	0.4585	0.081	0.1235	0.9845

qubit are $R_{\text{GHZ}} = R_{\text{WState}} = [18, 26]$, $R_{\text{DJ}} = [14, 22]$, and $R_{\text{QFT}} = [10, 18]$, where smaller ranges are assigned to QFT and DJ to account for their higher connectivity requirements. In Scenario 2 (Sc.2), increased qubit demand is considered by shifting each range upward by 4, giving $R_{\text{GHZ}} = R_{\text{WState}} = [22, 30]$, $R_{\text{DJ}} = [18, 26]$, and $R_{\text{QFT}} = [14, 22]$. For a given M , simulations are repeated over 10 independently generated \mathcal{QC} sets, and results are averaged across runs.

The linear regression model is implemented using the `scikit-learn` library and a dataset covering all four circuit types with $w_m \in [10, 30]$. The cut size for k -way partitioning, $\text{Cut}_m^{(k)}$ in (4), is obtained by iteratively applying the K-L algorithm in `NetworkX` [33] until the desired number of partitions are obtained. The partitioning cost ν_{mk} is computed using the linear model in (5), with connectivity features γ_m , $\lambda_{2,m}$, and σ_m/g_m extracted from each circuit's graph. The regression coefficients and R^2 scores are reported in Table II, which indicate good predictive performance. Among the features, $\lambda_{2,m}$ is the most influential, while the coefficients for γ_m and σ_m/g_m are smaller but tend to increase with higher partition counts k .

The proposed scheduling methods (Algorithms 1 and 4) are implemented in Python. The parameter β in the batch selection process of Algorithm 1 is set to 0.85, and the partition count threshold K_m^{\max} is fixed at 4 for all circuits. The MILP optimisation problems defined in Problem Formulations 1 and 2 are solved using the `Python-MIP` package with the Gurobi optimiser. After obtaining the optimal assignment, each quantum circuit is partitioned individually using the K-L algorithm, which determines both the number of remote gates between each QPU pair allocated to a given circuit and the total number of remote gates for that circuit.

To evaluate the performance of the proposed scheduling methods, we consider several key figures of merit. All results are averaged over repeated simulation runs. We choose random scheduling as the baseline for comparison.

- **Number of remote gates per QCirc:** the total number of remote gates across all M QCircs, divided by M .
- **Number of circuit partitions per QCirc:** the total number of circuit partitions across all M QCircs, divided by M .
- **Normalised Job Execution Time (JET) for each QCirc type:** Average execution time for a given QCirc type, computed over all its occurrences within \mathcal{QC} and normalised by T_{dec} , i.e., $\text{JET}/T_{\text{dec}}$.
- **Number of remote gates for each QCirc type:** Average number of remote gates for a given QCirc type, computed over all its occurrences within \mathcal{QC} .
- **Normalised Makespan:** the total time required to com-

plete all jobs (i.e., the execution of all M QCircs), normalised by T_{dec} , for consistency with normalised JET and to ensure hardware platform independence.

- **Normalised Throughput:** defined as the ratio of the number of QCircs (M) to Normalised Makespan. This indicates how many QCircs can be executed per unit time.

The normalised JET for a specific QCirc is obtained using the `Qiskit` framework [34], which represents the circuit as a sequence of layers, where each layer comprises quantum gates that can be executed in parallel. The execution time is calculated under the following conditions. First, we assume that remote gates within a layer of a given QCirc are executed sequentially rather than in parallel. Second, all local gates are assumed to have an identical execution duration. Based on these, we iterate through all circuit layers and identify whether each layer contains any remote gates or only local gates. Let N_{LL} denote the number of layers containing only local gates. We compute the normalised JET using the following expression:

$$\frac{\text{JET}}{T_{\text{dec}}} = N_{\text{LL}} \frac{T_{\text{local}}}{T_{\text{dec}}} + \sum_{n_s \in \{1, 3, 5\}} N_{\text{link}_{n_s}}^{(rg)} \frac{T_{\text{link}_{n_s}}}{T_{\text{dec}}} \quad (8)$$

where $N_{\text{link}_{n_s}}^{(rg)}$ denotes the number of remote gates in the QCirc under consideration that are executed across the links with n_s optical switches. In all simulations and calculations, we assume $T_{\text{local}}/T_{\text{dec}} = 5 \times 10^{-4}$ and $T_{\text{el}}/T_{\text{dec}} = 0.005$.

Fig. 7 and 8 present the average number of remote gates and circuit partitions per QCirc, respectively, for the proposed scheduling methods, compared against random scheduling as the baseline. The results are shown for qubit-range schemes Sc.1 and Sc.2 used in our simulations. For the Batch-QCirc scheduling method, several values of the parameter α (fraction threshold of the total qubits across all QPUs available before executing the next batch) are considered. As shown, both the Batch-QCirc and Single-QCirc methods result in a lower number of remote gates and, consequently, require fewer partitions for each QCirc compared to the baseline. Moreover, in all cases, the Batch-QCirc method outperforms the Single-QCirc approach with a more complex MILP optimisation process. The number of remote gates directly reflects the demand for communication resources between QPUs. Therefore, the results demonstrate that both proposed methods, and especially the Batch-QCirc assignment, effectively reduce inter-QPU communication overhead.

In our simulations, we also obtained the number of remote gates for all four evaluated circuit types individually within the set of circuits \mathcal{QC} . The overall results followed a similar pattern to those of JET (presented in Fig. 9)), as it also can be expected from Eq. (8). Therefore, for the sake of brevity, we do not include the results for all cases here, but present the results for the specific case with the total number of QCircs (M) equal to 36 in Table III. For QFT when the total number of qubits required is low (in the range of 10–18 in Sc.1), the proposed Batch-QCirc assignment typically assigns QFT to a single QPU rather than distributing it across multiple QPUs, resulting in an average of zero remote gates. When the qubit

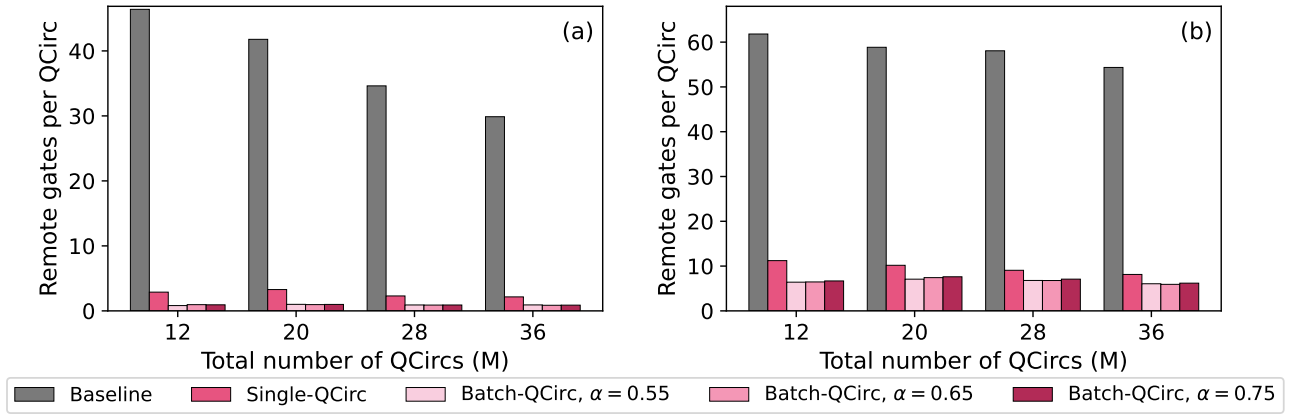


Fig. 7. Average number of remote gates in DQC divided by the total number of QCircs M , for the proposed and baseline scheduling methods. (a) Qubit-range scheme Sc.1, (b) Qubit-range scheme Sc.2.

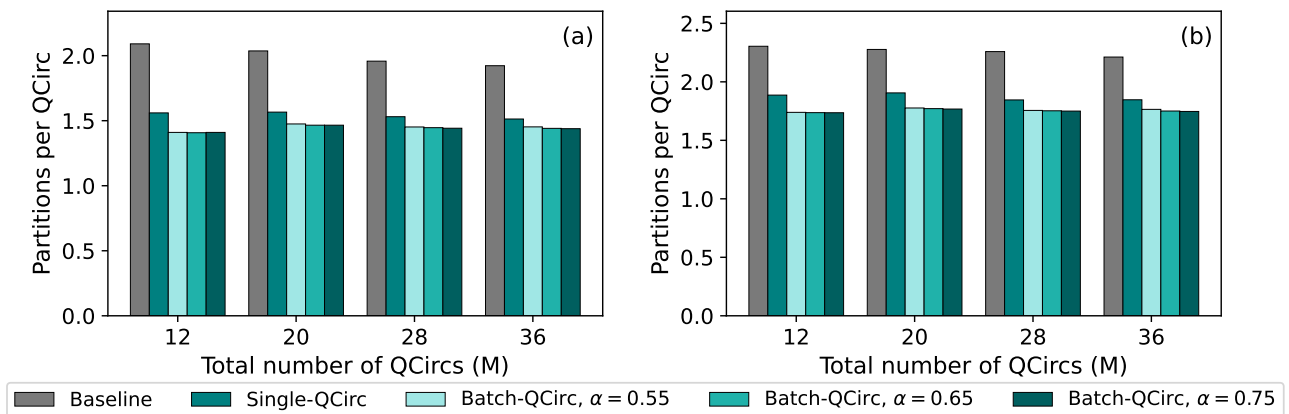


Fig. 8. Average number of circuit partitions divided by the total number of QCircs M , for the proposed and baseline scheduling methods. (a) Qubit-range scheme Sc.1, (b) Qubit-range scheme Sc.2.

TABLE III
AVERAGE NUMBER OF REMOTE GATES FOR EACH QCIRC TYPE
UNDER THE TWO QUBIT-RANGE SCHEMES SC.1 AND SC.2.

	Baseline		Single-QCirc		Batch-QCirc ($\alpha = 0.55$)		Batch-QCirc ($\alpha = 0.65$)		Batch-QCirc ($\alpha = 0.75$)	
	Sc.1	Sc.2	Sc.1	Sc.2	Sc.1	Sc.2	Sc.1	Sc.2	Sc.1	Sc.2
QFT	106.3	199.4	4.37	24.76	0	16.65	0	16.1	0	17.3
DJ	9.6	13.74	1.92	4.53	1.36	4.41	1.17	4.45	1.25	4.3
W-State	2.37	2.83	1.56	2.18	1.5	2.08	1.17	2.08	1.25	2.09
GHZ	1.18	1.39	0.76	1.07	0.81	1.08	0.8	1.06	0.8	1.04

demand is increased in Sc.2, however, the number of remote gates rises significantly across all scheduling methods.

Next, we evaluate the normalised Job Execution Time (JET), obtained for each circuit type individually. As shown in Fig. 9, the proposed methods consistently outperform the baseline with reduced execution times across all QCirc types. Batch-QCirc scheduling further improves JET in most cases compared to the Single-QCirc approach. For Sc.1, Batch-QCirc significantly reduces the normalised JET of QFT (to about 0.0145) by executing it locally within a single QPU. With higher qubit demand in Sc.2, QFT (Fig. 9(e)) and DJ (Fig. 9(f)) exhibit higher JET than W-state (Fig. 9(g)) and GHZ (Fig. 9(h)), reflecting their greater connectivity, which

induces more remote gates and hence longer execution times. In joint-optimisation-based Batch-QCirc scheduling, reducing the JET of highly connected circuits tends to prioritise QPUs with greater capacity, improving fidelity and reducing communication links, but limiting optimisation for less connected circuits such as GHZ. This trade-off is evident in both Sc.1 and Sc.2, where Single-QCirc sometimes yields lower JET for GHZ. Such interdependence highlights the system-level nature of Batch-QCirc scheduling, where resource trade-offs naturally arise.

Overall, these results demonstrate the effectiveness of the proposed methods in reducing the execution time of quantum circuits compared to the baseline. This improvement is particularly notable for circuits with a highly connected structure, such as the QFT circuits in our simulations. Under random scheduling, the normalised JET (i.e., JET/T_{dec}) often exceeds 1, meaning that a successful execution may require many trial rounds or may even become infeasible due to qubit decoherence. By applying the proposed methods, this ratio is significantly reduced, enabling more reliable circuit execution within coherence time constraints.

Next, we examine the normalised makespan and throughput, key metrics for efficient scheduling and resource management, with results shown in Fig. 10 and Fig. 11. The proposed

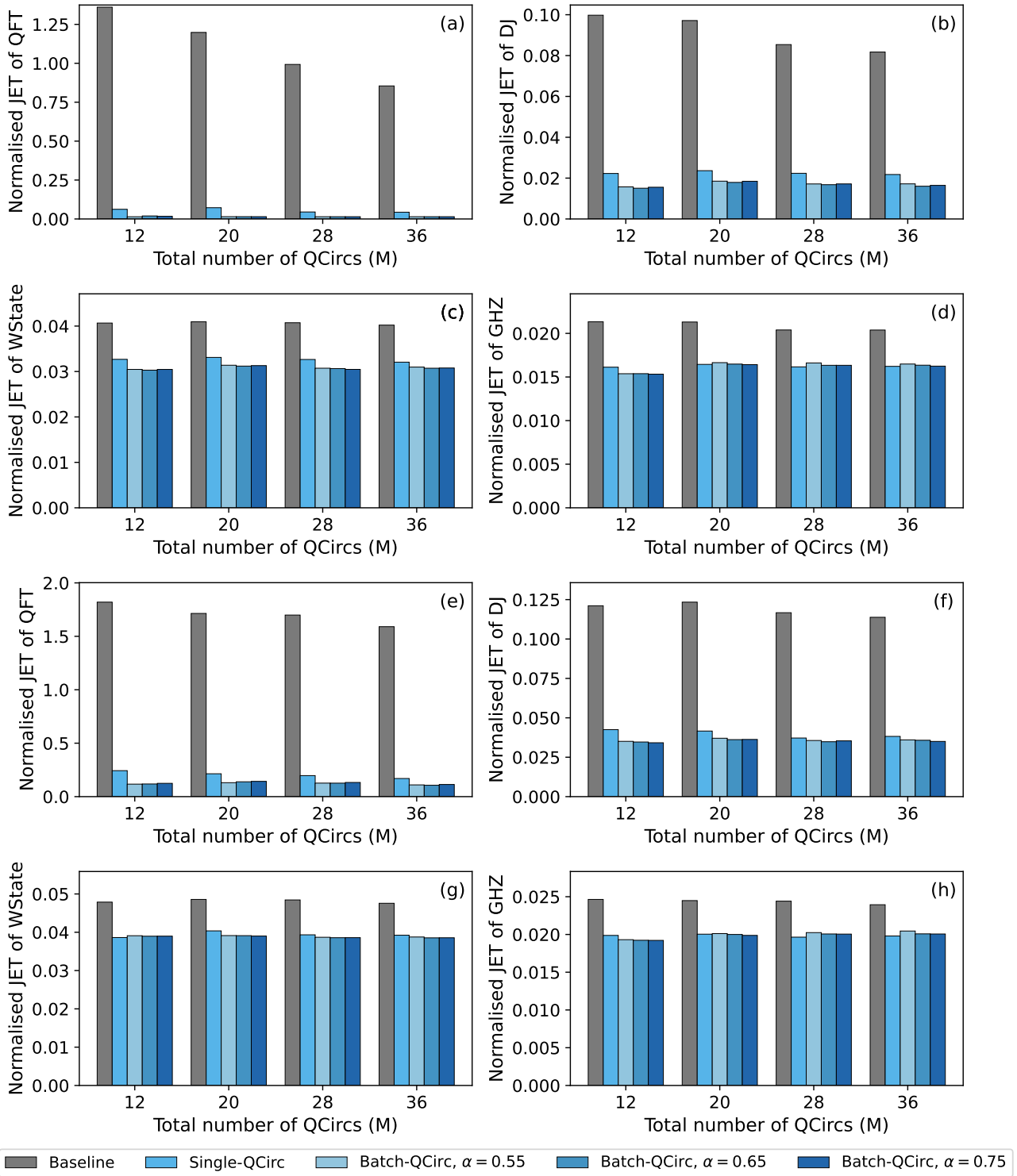


Fig. 9. Average Job Execution Time (JET) (normalised by T_{dec}) for the proposed and baseline scheduling methods across different circuit types. (a)–(d) Qubit-range scheme Sc.1, (e)–(h): Qubit-range scheme Sc.2.

methods significantly improve both metrics, with the Batch-QCirc approach outperforming the Single-QCirc method. This demonstrates the system-level effectiveness of Batch-QCirc scheduling: reductions in JET due to fewer remote gates translate directly into shorter makespan and higher throughput.

We also compare Batch-QCirc scheduling with varying values of α , examining all the results presented in this

section. In terms of makespan and throughput, the Batch-QCirc scheduling with $\alpha = 0.75$ consistently results in a slightly worse performance compared to other values. Since the parameter α determines when the algorithm proceeds to the next scheduling cycle, it plays a crucial role in affecting these evaluated metrics. For the results of average number of remote gates and JET, similarly, $\alpha = 0.75$ does not show

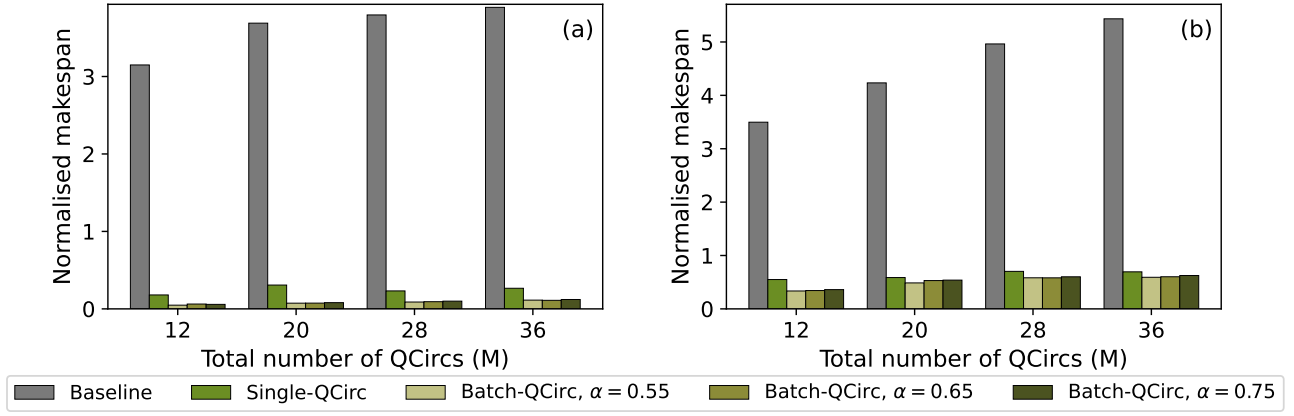


Fig. 10. Average makespan (normalised by T_{dec}) for the proposed and baseline scheduling methods. (a) Qubit-range scheme Sc.1, (b) Qubit-range scheme Sc.2.

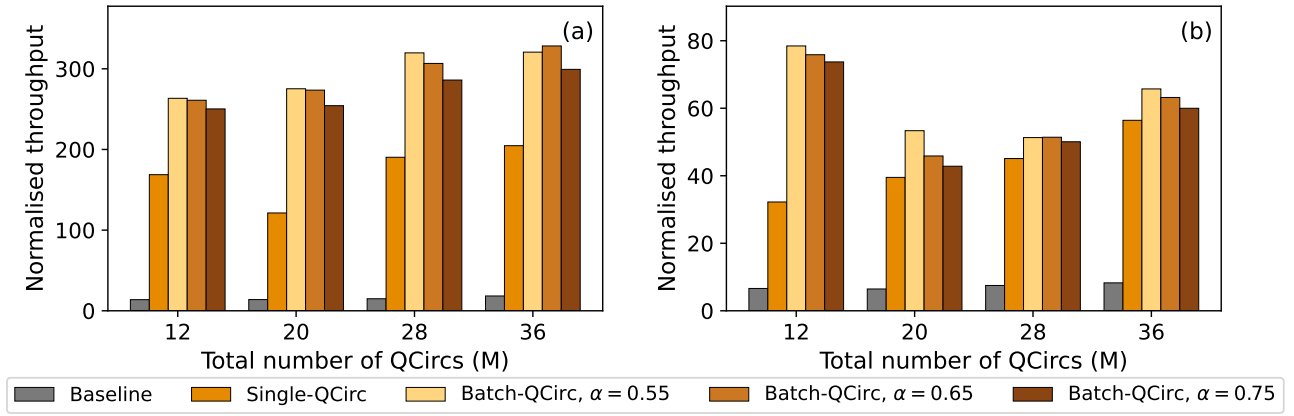


Fig. 11. Average throughput (normalised by T_{dec}) for the proposed and baseline scheduling methods. (a) Qubit-range scheme Sc.1, (b) Qubit-range scheme Sc.2.

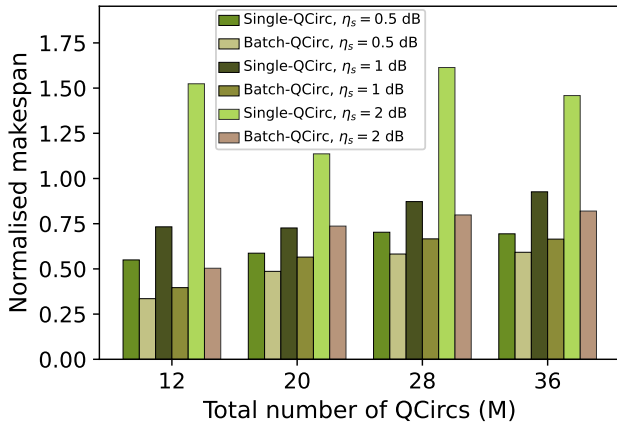


Fig. 12. Average makespan (normalised by T_{dec}) for Single-QCirc and Batch-QCirc ($\alpha = 0.55$) scheduling methods under varying optical switch loss, assuming the qubit-range scheme Sc.2.

meaningful improvements over $\alpha = 0.55$ or $\alpha = 0.65$; In fact, the latter two often outperform $\alpha = 0.75$. These results indicate that increasing waiting time for scheduling the next batch with a higher α may lead to unnecessary resource waste without performance gains.

Lastly, to investigate the impact of optical switch on the performance of the proposed DQC scheme, we increase the optical switch loss, which consequently raises the average entanglement generation time - $T_{link_1}, T_{link_3}, T_{link_5}$. Fig. 12 presents the makespan results for the single-QCirc and batch-QCirc ($\alpha = 0.55$) methods under varying optical switch losses, $\eta_s = 0.5$ dB, 1 dB, and 2 dB, assuming the qubit-range scheme Sc.2. The results demonstrate that as η_s increases, the relative advantage of Batch-QCirc becomes more pronounced. For instance, for $M = 36$, Batch-QCirc reduces the makespan by 14.7% compared to Single-QCirc at $\eta_s = 0.5$ dB, with the improvement increasing to 28.3% and 43.8% at $\eta_s = 1$ dB and $\eta_s = 2$ dB, respectively. These results highlight the particular promise of the Batch-QCirc approach in topologies with heterogeneous link qualities.

V. CONCLUSION

In this work, we address the challenge of efficient resource management and QCirc scheduling in distributed quantum computing networks. We propose two scheduling approaches: a dynamic Batch-QCirc scheduling method, which operates through sequential scheduling cycles with batch optimisation, and a Single-QCirc scheduling method that optimises QCirc allocation individually. To achieve optimal assignment

of QCircs to QPUs, we developed MILP formulations that minimise errors arising from inter-QPU communication. These formulations also account for network topology, link loss, QPU capacities, and QCirc structure in the DQC, enabling effective and quantum resource-aware assignment. We combine both approaches with quantum circuit partitioning and evaluate their performance through extensive simulations, showing that our methods support reliable QCirc execution while improving overall resource utilisation.

This work takes an initial step toward quantum- and network-aware job scheduling in cloud-based quantum data centres, incorporating quantum-specific features and network considerations. Future work will explore priority- and time-aware scheduling, advanced learning models, and reinforcement learning for adaptive, scalable algorithms, paving the way for intelligent resource management in quantum cloud infrastructures.

ACKNOWLEDGMENT

The authors would like to express their sincere gratitude to Reza Nejabati for his support and insightful technical discussions.

REFERENCES

- [1] D. Cuomo, M. Caleffi, and A. S. Cacciapuoti, "Towards a distributed quantum computing ecosystem," *IET Quantum Communication*, vol. 1, no. 1, pp. 3–8, 2020.
- [2] M. Caleffi *et al.*, "Distributed quantum computing: a survey," *arXiv preprint arXiv:2212.10609*, 2022.
- [3] A. Yimsiriwattana and S. J. Lomonaco Jr, "Distributed quantum computing: A distributed shor algorithm," in *Quantum Information and Computation II*, vol. 5436. SPIE, 2004, pp. 360–372.
- [4] D. Barral, F. J. Cardama, G. Diaz-Camacho, D. Fafalde, I. F. Llovo, M. Musso-Juane, J. Vázquez-Pérez, J. Villasuso, C. Piñeiro, N. Costas *et al.*, "Review of distributed quantum computing: from single qpu to high performance quantum computing," *Computer Science Review*, vol. 57, p. 100747, 2025.
- [5] K. Campbell, A. Lawey, and M. Razavi, "Quantum data centres: a simulation-based comparative noise analysis," *Quantum Science and Technology*, vol. 10, no. 1, p. 015052, 2024.
- [6] M. Maronese, L. Moro, L. Rocutto, and E. Prati, "Quantum compiling," in *Quantum Computing Environments*. Springer, 2022, pp. 39–74.
- [7] Y. Shi, P. Gokhale, P. Murali, J. M. Baker, C. Duckering, Y. Ding, N. C. Brown, C. Chamberland, A. Javadi-Abhari, A. W. Cross *et al.*, "Resource-efficient quantum computing by breaking abstractions," *Proceedings of the IEEE*, vol. 108, no. 8, pp. 1353–1370, 2020.
- [8] A. Hussain, M. Aleem, A. Khan, M. A. Iqbal, and M. A. Islam, "RALBA: a computation-aware load balancing scheduler for cloud computing," *Cluster Computing*, vol. 21, pp. 1667–1680, 2018.
- [9] S. Singhal and A. Sharma, "Resource scheduling algorithms in cloud computing: A big picture," in *2021 5th International Conference on Information Systems and Computer Networks (ISCON)*. IEEE, 2021, pp. 1–6.
- [10] S. K. Mishra, B. Sahoo, and P. P. Parida, "Load balancing in cloud computing: a big picture," *Journal of King Saud University-Computer and Information Sciences*, vol. 32, no. 2, pp. 149–158, 2020.
- [11] O. Elzeki, M. Rashad, and M. A. Elsoud, "Overview of scheduling tasks in distributed computing systems," *International Journal of Soft Computing and Engineering*, vol. 2, no. 3, pp. 470–475, 2012.
- [12] R. D. Oliveira, S. Bahrani, E. Arabul, R. Wang, R. Nejabati, and D. Simeonidou, "FPGA-based deterministic and low-latency control for distributed quantum computing," in *IEEE INFOCOM 2023-IEEE Conference on Computer Communications Workshops (INFOCOM WKSHPS)*. IEEE, 2023, pp. 1–6.
- [13] F. Vista, S. DiAdamo, E. Kaur, H. Shapourian, and R. Nejabati, "Entanglement request scheduling in quantum datacenter networks," *IEEE Network*, 2025.
- [14] H. Zhang, Y. Xu, H. Hu, K. Yin, H. Shapourian, J. Zhao, R. R. Kompella, R. Nejabati, and Y. Ding, "Switchqnet: Optimizing distributed quantum computing for quantum data centers with switch networks," in *Proceedings of the 52nd Annual International Symposium on Computer Architecture*, 2025, pp. 1449–1463.
- [15] S. Pouryousef, R. Nejabati, D. Towsley, R. Kompella, and E. Kaur, "Network-aware scheduling for remote gate execution in quantum data centers," *arXiv preprint arXiv:2504.20176*, 2025. [Online]. Available: <https://arxiv.org/abs/2504.20176>
- [16] C. Cicconetti, M. Conti, and A. Passarella, "Resource allocation in quantum networks for distributed quantum computing," in *2022 IEEE International conference on smart computing (SMARTCOMP)*. IEEE, 2022, pp. 124–132.
- [17] D. Ferrari, A. S. Cacciapuoti, M. Amoretti, and M. Caleffi, "Compiler design for distributed quantum computing," *IEEE Transactions on Quantum Engineering*, vol. 2, pp. 1–20, 2021.
- [18] D. Cuomo, M. Caleffi, K. Krsulich, F. Tramonto, G. Agliardi, E. Prati, and A. S. Cacciapuoti, "Optimized compiler for distributed quantum computing," *ACM Transactions on Quantum Computing*, vol. 4, no. 2, pp. 1–29, 2023.
- [19] D. Ferrari, S. Carretta, and M. Amoretti, "A modular quantum compilation framework for distributed quantum computing," *IEEE Transactions on Quantum Engineering*, 2023.
- [20] O. Daei *et al.*, "Optimized quantum circuit partitioning," *International Journal of Theoretical Physics*, vol. 59, no. 12, pp. 3804–3820, 2020.
- [21] W. Cambiucci *et al.*, "Hypergraphic partitioning of quantum circuits for distributed quantum computing," *arXiv preprint arXiv:2301.05759*, 2023.
- [22] P. Andres-Martinez *et al.*, "Automated distribution of quantum circuits via hypergraph partitioning," *Physical Review A*, vol. 100, no. 3, p. 032308, 2019.
- [23] Z. Davarzani, M. Zomorodi-Moghadam, M. Houshmand, and M. Nouri-Baygi, "A dynamic programming approach for distributing quantum circuits by bipartite graphs," *Quantum Information Processing*, vol. 19, pp. 1–18, 2020.
- [24] E. Kaur, H. Shapourian, J. Zhao, M. Kilzer, R. Kompella, and R. Nejabati, "Optimized quantum circuit partitioning across multiple quantum processors," in *Quantum Computing, Communication, and Simulation V*, vol. 13391. SPIE, 2025, pp. 152–156.
- [25] D. Dadkhah, M. Zomorodi, and S. E. Hosseini, "A new approach for optimization of distributed quantum circuits," *International Journal of Theoretical Physics*, vol. 60, pp. 3271–3285, 2021.
- [26] P. Andres-Martinez, T. Forrer, D. Mills, J.-Y. Wu, L. Henaut, K. Yamamoto, M. Murao, and R. Duncan, "Distributing circuits over heterogeneous, modular quantum computing network architectures," *arXiv preprint arXiv:2305.14148*, 2023.
- [27] R. Parekh *et al.*, "Quantum algorithms and simulation for parallel and distributed quantum computing," in *2021 IEEE/ACM Second International Workshop on Quantum Computing Software (QCS)*. IEEE, 2021, pp. 9–19.
- [28] H. Shapourian *et al.*, "Quantum data center infrastructures: A scalable architectural design perspective," *arXiv preprint arXiv:2501.05598*, 2025.
- [29] J. Ang, G. Carini, Y. Chen, I. Chuang, M. Demarco, S. Economou, A. Eickbusch, A. Faraon, K.-M. Fu, S. Girvin *et al.*, "Arquin: architectures for multinode superconducting quantum computers," *ACM Transactions on Quantum Computing*, vol. 5, no. 3, pp. 1–59, 2024.
- [30] H. Beukers, M. Pasini, H. Choi, D. Englund, R. Hanson, and J. Borregaard, "Tutorial: Remote entanglement protocols for stationary qubits with photonic interfaces (2023)," *arXiv preprint arXiv:2310.19878*.
- [31] M. Fiedler, "Algebraic connectivity of graphs," *Czechoslovak Mathematical Journal*, vol. 23, no. 2, pp. 298–305, 1973.
- [32] N. Quetschlich, L. Burgholzer, and R. Wille, "MQT Bench: Benchmarking software and design automation tools for quantum computing," *Quantum*, 2023, MQT Bench is available at <https://www.cda.cit.tum.de/mqtbench/>.
- [33] A. A. Hagberg, D. A. Schult, and P. J. Swart, "Exploring network structure, dynamics, and function using networkx," in *Proceedings of the 7th Python in Science Conference*, G. Varoquaux, T. Vaught, and J. Millman, Eds., Pasadena, CA USA, 2008, pp. 11 – 15.
- [34] A. Javadi-Abhari, M. Treinish, K. Krsulich, C. J. Wood, J. Lishman, J. Gacon, S. Martiel, P. D. Nation, L. S. Bishop, A. W. Cross, B. R. Johnson, and J. M. Gambetta, "Quantum computing with Qiskit," *arXiv preprint arXiv:2405.08810*, 2024. [Online]. Available: <https://arxiv.org/abs/2405.08810>